Nat. Hazards Earth Syst. Sci. Discuss., 2, 3351–3395, 2014
www.nat-hazards-earth-syst-sci-discuss.net/2/3351/2014/
doi:10.5194/nhessd-2-3351-2014

Natural Hazards and Earth System Sciences
Discussions
Open Access

Simulating lightning into the RAMS model: implementation and preliminary results

S. Federico[1], E. Avolio[2], M. Petracca[1], G. Panegrossi[1], P. Sanò[1], D. Casella[1], and S. Dietrich[1]

[1]ISAC-CNR, UOS of Rome, via del Fosso del Cavaliere 100, 00133-Rome, Italy
[2]CRATI, c/o University of Calabria, 87032 Rende (CS), Italy

Received: 14 March 2014 – Accepted: 26 April 2014 – Published: 12 May 2014

Correspondence to: G. Panegrossi (g.panegrossi@isac.cnr.it)

Published by Copernicus Publications on behalf of the European Geosciences Union.

Abstract

This paper shows the results of a tailored version of a previously published methodology, designed to simulate lightning activity, implemented into the Regional Atmospheric Modeling System (RAMS).

The method gives the flash density at the resolution of the RAMS grid-scale allowing for a detailed analysis of the evolution of simulated lightning activity.

The system is applied in detail to two case studies occurred over the Lazio Region, in Central Italy. Simulations are compared with the lightning activity detected by the LINET network. The cases refer to two thunderstorms of different intensity.

Results show that the model predicts reasonably well both cases and that the lightning activity is well reproduced especially for the most intense case. However, there are errors in timing and positioning of the convection, whose magnitude depends on the case study, which mirrors in timing and positioning errors of the lightning distribution.

To assess objectively the performance of the methodology, standard scores are presented for four additional case studies. Scores show the ability of the methodology to simulate the daily lightning activity for different spatial scales and for two different minimum thresholds of flash number density. The performance decreases at finer spatial scales and for higher thresholds.

The comparison of simulated and observed lighting activity is an immediate and powerful tool to assess the model ability to reproduce the intensity and the evolution of the convection. This shows the importance of the use of computationally efficient lightning schemes, such as the one described in this paper, in forecast models.

1 Introduction

The lightning threat in convective thunderstorms is a significant concern for the public safety (Curran et al., 2000) and for activities that are sensitive to this threat, as aviation and management of electric infrastructures.

Lightning is a characteristic of severe weather and often accompanies heavy precipitation and large hail. The relationship between lightning and heavy precipitation has been studied extensively in several parts of the world (Tapia et al., 1998; Land and Rutledge, 2002; Latham et al., 2003; Soula et al., 1998; Zhou et al., 2002).

Gungle and Krider (2006) presented tables summarizing numerous previous studies that tried to derive the relationships of precipitation volume per cloud-to-ground (CG) lightning flash from different sensors, such as rain gauges and radars. This relationship varies from site to site, and from sea to land, showing that the lightning activity largely depends on the geographical and climate conditions. The lag time between lightning and surface rainfall varied from 4–20 min based on rain gauges to less than 10 min based on radar.

In the Mediterranean region the relationship between lightning and precipitation has also been studied, based on satellite (Tropical Rainfall Measuring Mission (TRMM) Lightning Image Sensor (LIS); Cecil et al., 2005; Goodman et al., 2007), and ground-based lightning location systems (Altaratz et al., 2003; Defer et al., 2005; Price and Federmesser, 2006; Katsanos et al., 2007a, b). The FLASH project (Price et al., 2011) aimed at improving the understanding and forecasting ability of flash floods in the Mediterranean region using lightning data. It was found that real-time lightning observations on a regional basis are very useful in detecting, monitoring and tracking intense thunderstorm activity on large spatial scales.

These studies confirm that the lightning is related to deep convection and heavy rains. However, as pointed out by Petersen et al. (2005), while the relationship between rainfall and lightning is highly regime dependent and there is a large variability of the water volume/flash found in different areas of the world, the relationship between total lightning activity and ice mass is more robust. In their study they found that, on a global scale, the relationship between column integrated precipitation ice mass and lightning flash density is invariant between land, ocean, and coastal regimes (in contrast to rainfall), suggesting that the physical assumptions of precipitation-based charging and mixed phase precipitation development are robust.

Deierling et al. (2008a, b) used a Doppler and dual-polarimetric radar as a source of information of ice distribution and updraft in clouds, and lightning data collected in Northern Alabama and Colorado/Kansas during two field campaigns. They showed that the updraft volume in the charging zone was highly correlated with total lightning activity, finding that these relationships are relatively invariant between different climate conditions.

It should also be mentioned that the lightning activity has an influence on atmospheric chemistry because of its ability to create nitrogen oxides (e.g. Grewe, 2009).

All those subjects foster the interest in observing and forecasting lightning, as confirmed by the planned launch of a Geostationary Lightning Mapper aboard GOES-R satellites and of the Lightning Imager on METEOSAT Third Generation (MTG), and the increasing interest for ground-based lightning detection networks. Moreover, there has been an increasing interest in investigating more in detail the mechanisms of the electrification processes, in order to find quantitative relationships between lightning flashes and cloud properties directly connected with them, such as precipitating and non-precipitating ice mass content, and cloud updrafts. In order to do that, cloud electrification models are used.

Nowadays, the methods to simulate lightning in thunderstorm may be classified in two main groups. The first contains advanced one-dimensional (Solomon and Baker, 1996; Solomon et al., 2005; Formenton et al., 2013) or three-dimensional (Mansell et al., 2002, 2005; MacGormam et al., 2001) cloud models equipped with sophisticated electrification schemes. These schemes make use of the results of laboratory experiments, which have revealed the transfer of charge during hydrometeor collisions (Saunders, 2008, reviews the mechanisms of charge separation in thunderstorms). In these methods the electric field and the dielectric breakdown are explicitly simulated.

These schemes were also parameterized in cloud resolving and mesoscale models (Mansell et al., 2005; Barthe et al., 2005). Recently, Lynn et al. (2012) implemented a dynamically based algorithm into the WRF model to produce forecast maps for positive and negative cloud-to-ground and intra cloud lightning. Their methodology uses the

NHESSD
2, 3351–3395, 2014

dynamic and microphysics fields from WRF to calculate the electrical potential energy for positive and negative cloud-to-ground, and intra cloud lightning, adding prognostic equations for three variables in the WRF model. The number of cloud-to-ground (positive and negative) and intra cloud lightning is computed from these potentials, whenever the potential energy is larger than a threshold energy, whose value depends on the type of lightning (positive and negative cloud-to-ground and intra cloud). Scores for seven case studies indicate that the methodology is able to predict the occurrence of the positive and negative cloud-to-ground and intra cloud events.

The second group contains simple schemes that correlate the hydrometeors or other parameters computed by cloud resolving models (nowadays with horizontal resolution ≤ 3 km) with the number of observed flashes, giving the flash rate (Price and Rind, 1992; McCaul et al., 2009; Yoshida et al., 2009; Yair et al., 2010; Wong et al., 2013). Wong et al. (2013), revised the Price and Rind (1992) parameterizations by applying the methodology in cloud resolving models. They showed the need for a validation and tuning of the parameterizations when applying the method to cloud resolving models.

These schemes have the advantage to be simple and computationally efficient, giving a tool for implementing the lightning forecast operationally. Moreover, several of the above mentioned papers show the superiority of these schemes compared to a former generation of methods that have been based on the correlation between thunderstorm occurrence and thermodynamic indices (e. g. Bright et al., 2004).

Several other studies confirm the good relationship between the lightning activity and the solid hydrometeors, which are usually used in the lightning scheme of cloud resolving models. Katsanos et al. (2007a, b) carried out a study on the relationship between lightning activity reported by the ZEUS lightning detection network, and microphysical parameters of clouds simulated with the non-hydrostatic MM5 model, for a number of cases over the central and eastern Mediterranean. The analysis showed that the temporal distribution of lightning is not well correlated with convective rainfall, while it is well correlated with the simulated concentrations of solid hydrometeors.

This paper shows the implementation of a methodology to simulate lightning activity in the RAMS model and shows the results of its application to six case studies in Central Italy. Two of these cases are analysed in detail, while statistical scores are presented for all cases. The method used in this study belongs to the second group of methods to simulate lightning in cloud resolving models described above, because it is rather simple and computationally efficient.

The approach is a tailored form of the method of Dahl et al. (2011a, b), hereafter DHS1 and DHS2. In particular DHS1 shows the theoretical underpinnings of the scheme implemented and the reader should refer to this work for a detailed discussion of the physical foundation of the methodology, while DHS2 discusses its practical implementation in the COSMO (Consortium for Small Scale Modeling) model.

The methodology presented in this paper differs from DHS1 and DHS2 because it is designed to account for the differences of RAMS with respect to the COSMO model and to focus on the charge separation processes occurring in the charging zone, and it also uses a different method to spatially distribute the simulated lightning associated to the convective cells.

The paper is organized as follows: in Sect. 2 the RAMS model is introduced, as well as the details of the methodology used in this work, and the lightning detection network used for comparison with the model results. Section 3 shows in detail the results of two case studies occurred over the Lazio Region, in central Italy, as well as the scores for these two cases. To make the results statistically more robust, and to define better the limits of applicability of the methodology presented in this paper, scores of four additional cases are also shown. The discussion and conclusions are provided in Sect. 4.

NHESSD
2, 3351–3395, 2014

2 Materials and methods

2.1 The RAMS model configuration

The events considered in this paper are studied using the RAMS model (non-hydrostatic), version 6.0. A detailed description of the RAMS model is given in Cotton et al. (2003) while the following is a brief description of the model setup. The RAMS model is also used operationally in southern Italy (Federico, 2011).

Two two-way nested domains at 10 km and 2.5 km horizontal resolutions respectively, are used (Table 1, Fig. 1). Thirty-five vertical levels, up to 21 800 m in the terrain-following coordinate system, are used for both domains. Levels are not equally spaced: layers within the Planetary Boundary Layer (PBL) are between 50 and 200 m thick, whereas layers in the middle and upper troposphere are 1000 m thick.

The Land Ecosystem-Atmosphere Feedback model (LEAF) is used to calculate the exchange between soil, vegetation, and atmosphere (Walko et al., 2000). LEAF is a representation of surface features, including vegetation, soil, lakes and oceans, and snow cover, and their influence on each other and on the atmosphere.

Explicitly resolved precipitation is computed from bulk microphysics prognostic equations for the mixing ratio of seven water categories: cloud water, rain, pristine ice, snow, aggregates, graupel, and hail (Walko et al., 1995). Snow, aggregates, and pristine ice are assumed completely frozen, cloud water and rain are liquid water, while graupel and hail are mixed-phase categories. The scheme uses a generalized gamma size-spectrum, rather than a Marshall–Palmer, and uses a stochastic collection rather than a continuous accretion. The scheme includes a heat budget equation for each hydrometeor class, allowing heat storage and the existence of mixed phase hydrometeors.

Sub-grid-scale effect of convective and non-convective clouds is parameterized following Molinari and Corsetti (1985) who proposed a simplified form of the Kuo scheme (Kuo, 1974) that accounts for updrafts and downdrafts. RAMS parameterizes the unresolved transport using K-theory, in which the covariance is evaluated as the product of an eddy mixing coefficient and the gradient of the transported quantity. The turbu-

NHESSD
2, 3351–3395, 2014

lent mixing in the horizontal directions is parameterized following Smagorinsky (1963), which relates the mixing coefficients to the fluid strain rate and includes corrections for the influence of the Brunt-Vaisala frequency and the Richardson number (Pielke, 2002). A full-column, two-stream single-band radiation scheme is used to calculate short-wave and long-wave radiation (Chen and Cotton, 1983). The Chen and Cotton scheme accounts for condensate in the atmosphere, but not whether it is cloud water, rain, or ice.

Detailed information on the initial and dynamic boundary conditions is given in Sect. 3.

2.2 Lightning simulation

The method to calculate the lightning distribution from the meteorological model output is tailored from the works of DHS1 and DHS2. The method assumes a plane capacitor scheme and is based on the idea that the flash rate is not only determined by the charging rate, but also by the geometry-dependent discharge strength of each lightning flash. The flash rate is given by:

$$f = \gamma j \frac{A}{\Delta Q} \tag{1}$$

where f is the flash rate (s^{-1}), γ is the lightning efficiency (0.9), A is the area (m^2) of the plane plate capacitor, j ($C\,m^{-2}\,s^{-1}$) is the charging current, and $\Delta Q(C)$ is the averaged charge neutralized by the lightning.

For the application of this approach the geometrical properties of the capacitor need to be determined. These properties are formulated using the ice and graupel fields from the cloud resolving model and the idea underlying the parameterization is that the graupel contains the negative charge, while the ice has the positive charge. The charge is separated by the non-inductive graupel-ice mechanism (Saunders, 2008). In our formulation of the methodology, the ice field is given by the sum of pristine ice,

NHESSD
2, 3351–3395, 2014

snow and aggregates, while the graupel field is given by the sum of the graupel and hail hydrometeors.

The graupel region is identified by the region where the graupel concentration ($g\,m^{-3}$) is larger than $0.1\,g\,m^{-3}$ and the temperature is between 273 and 248 K. This limits the identification of the graupel cells into the charging zone. The ice region is identified by requiring its concentration larger than $0.1\,g\,m^{-3}$ and the temperature below 273 K.

In general, for an instantaneous output of the meteorological model, several ice and graupel cells are found. To identify them, the Hoshen and Kopelman (1976, see also DHS2) labelling algorithm is used. This method, which was originally developed in the percolation theory, is an efficient way for labelling as a "cell" a continuous field satisfying some properties (for example graupel concentration larger than $0.1\,g\,m^{-3}$ and temperature between 273 and 248 K). The percolation theory (Stauffer and Aharony, 1994) describes the behaviour of connected clusters in a random process. In our case, the clusters are composed by contiguous model grid boxes with graupel or ice density larger than $0.1\,g\,m^{-3}$, while the random process is the graupel and ice field of the RAMS model. During the last five decades, percolation theory has brought new understanding and techniques to a broad range of topics in physics, materials science, complex networks, epidemiology as well as in geology.

For each graupel cell, a centroid is identified and the area A (Eq. 1) of each graupel cell at the height of the centroid is determined. This area may cover several model grid boxes. Then it is verified that a graupel cell is topped by an ice cell. For this purpose the requirement is that that the area at the centroid of the graupel cell is topped by an ice cell by at least 70 % of its extension. By doing so the existence of a horizontal displacement between the graupel and ice regions in the thundercloud is allowed.

Once the geometrical properties of the graupel and ice regions are identified, the geometry of the plane capacitor is easily determined. In detail, its area A is given by the area of the graupel cells at the centroid height, while its volume V is found by multiplying the area A by the vertical distance between the ice and graupel centroids.

For each graupel cell the maximum graupel mass concentration (m_g) is found, which by definition is larger than $0.1\,\mathrm{g\,m^{-3}}$. The maximum graupel concentration and the geometry of the capacitor are the parameters needed to compute the flash rate of Eq. (1). In particular the discharge of each lightning is given by (DHS1):

$$\Delta Q = \begin{cases} 0.0 & \text{if } 0 < V \leq 2.5\,\mathrm{km^3} \\ 25[1-\exp(-0.013-0.027V)] & V > 2.5\,\mathrm{km^3} \end{cases} \tag{2}$$

where V is the volume of the capacitor associated with a thunderstorm cell.

The charging current is given by the charge density by the terminal velocity of the graupel, i.e. $j = \rho v_g$. The charge density ($\mathrm{C\,m^{-3}}$) is given by (DHS1):

$$\rho = \begin{cases} 0.0 & 0.0 \leq m_g < 0.1\,\mathrm{g\,m^{-3}} \\ 4.467\times10^{-10} + 3.067\times10^{-9} m_g & 0.1 \leq 3.0\,\mathrm{g\,m^{-3}} \\ 9.8\times10^{-9} & m_g > 3.0\,\mathrm{g\,m^{-3}} \end{cases} \tag{3}$$

To compute the terminal velocity of the graupel, the diameter of the graupel (D_g) is needed. It is given by (DHS1):

$$D_g(m_g) = \begin{cases} 0 & 0.0 \leq m_g < 0.1\,\mathrm{g\,m^{-3}} \\ 1.833\times10^{-3} + 3.333\times10^{-3} m_g & 0.1 \leq 3.0\,\mathrm{g\,m^{-3}} \\ 0.012 & \text{if } m_g > 3.0\,\mathrm{g\,m^{-3}} \end{cases} \tag{4}$$

Following Heymsfield and Kajikawa (1987) the terminal velocity of the graupel is found by $v_g = 422 D_g^{0.89}$.

NHESSD
2, 3351–3395, 2014

Once the flash rate (f_k) is determined for each kth thunderstorm cell, the lightning density $\rho_{\mathrm{fl}}(x,y,t)$ (number of flashes per unit area and per unit time) is computed as:

$$\begin{cases} \rho_k(x,y,t) = \begin{cases} f_k/A & x,y \in A \\ 0 & x,y \notin A \end{cases} \\ \rho_{\mathrm{fl}}(x,y,t) = \sum_{k=1}^{K} \rho_k(x,y,t) \end{cases} \tag{5}$$

where the k index spans the total number of discharging cells (K). The function $\rho_{\mathrm{fl}}(x,y,t)$ is defined on the same horizontal grid as the RAMS model and is updated at each call of the lightning scheme. The time interval between two calls of the lightning scheme is 10 min, which is a time scale appropriate to catch the convective development of the storms.

Therefore, in this study, the flashes are redistributed uniformly under the capacitor. The total number of flashes (N_{fl}) over a generic area S in the time interval Δt is given by the integral of the lightning density over the area S and time Δt, i.e.:

$$N_{\mathrm{fl}} = \int\limits_{\Delta t} \mathrm{d}t \int\limits_{S} \rho_{\mathrm{fl}}(x,y,t)\mathrm{d}S \tag{6}$$

Before concluding this section it should be noticed that, while the lightning scheme closely follows that of DHS1 and DHS2, there are some differences. The most significant are the following two:

a. The graupel cells are identified in the charging zone, which is identified as the layer between the 273 and 248 K isotherms (Saunders, 2008). DHS1 and DHS2 consider the region with temperatures below 263 K. We prefer the approach of this study because it considers explicitly the charging zone, where the charge separation process occurs.

b. The distribution of the lightning under the convective cell used in this paper follows more closely the shape of the convective cell compared to DHS2, which redistribute randomly the flashes in a circle centred at the thunderstorm cell centre and could develop unrealistic circular-shaped lightning patterns.

2.3 Lightning data

LINET (LIghtning detection NETwork; Betz et al., 2009) is a European lightning location network for high-precision detection of total lightning, ground strokes (exchanging charges between the cloud and the ground – CG cloud-to-ground) and cloud lightning (not making ground contact – IC intra cloud), with utilization of VLF/LF techniques (in range between 1 and 200 KHz). The network counts over 120 sensors in 17 European countries with a good coverage of the central and western Mediterranean (from 10° W to 35° E in longitude and from 30° N to 65° N in latitude).

Each LINET sensor consists of a crossed loop antenna for measuring the magnetic field, a GPS antenna for measuring the precise time reference and a PC for data acquisition. The lightning three-dimensional location is detected using the time of arrival (TOA) difference triangulation technique. The TOA method detects the horizontal and vertical position of lightning strokes that occur up to 100 km from the sensor itself. The system can measure the time (temporal resolution is about 512 ms), the horizontal and vertical location (with a position accuracy of 150 m for an average distance between sensors $\sim$ 200 km) of VLF-sources as well as the amplitude and the polarity of these events. The sensitivity thresholds is around 5 kA, but it depends on the location (Betz et al., 2009).

The accuracy for discrimination of ICs and CGs depends on the distance between the flash and the LINET sensors. However, since the approach used in this paper simulates the total lightning activity of thunderstorm, the total number of LINET strokes (IC+CG) registered at each location is used for comparison. The reported LINET "strokes" are grouped into "flashes" before the comparison with simulated flashes. For this purpose all events recorded by LINET that occur within 1 s and in an area with a radius of 10 km are binned into a single flash (Dahl et al., 2011b).

3 Results

In this section the results of two case studies over the Lazio Region (Central Italy) are firstly shown in detail, then the standard statistical scores for a total of six cases over the same area are analysed.

The first case study occurred on 20 October 2011 and was characterized by an intense lightning activity (16 231 flashes over Lazio for the whole day, see Table 2). The second occurred on 15 October 2012 and was characterized by a weaker lightning activity with 4820 flashes over Lazio for the whole day. These two cases represent a wide range of lightning activity over the region and, as evident from the results of the following sections, they also encompass a wide range of the lightning simulation performance. In particular, the performance of the model for the first case study is better than for the second case.

For the first case, the RAMS model is initialized at 12:00 UTC on 19 October 2011 and for the second case it is initialized at 12:00 UTC on 14 October 2012. Both simulations last 36 h. For both cases, the first 12 h are considered spin-up time and are discarded. Atmospheric initial and dynamic boundary conditions are derived from the European Centre for Medium Weather range Forecast (ECMWF) operational analyses. They are available every six hours at 0.25° horizontal resolution. A four-dimensional nudging technique is used to define the forcing at the lateral boundaries of the five outermost grid boxes of the largest domain.

For the first case (October 2011), sea surface temperature (SST) is interpolated onto the RAMS grids from OSI & SAF data (OSI & SAF, 2006), which are available at 00:00 UTC and 12:00 UTC. The horizontal resolution of the OSI & SAF field is 0.1°. Missing data are interpolated from neighbour data, using an inverse distance weighted average with a searching radius of 0.5°. The data are also averaged in time from the

NHESSD
2, 3351–3395, 2014

start time to the end of the simulation. The SST is held constant throughout the simulation. For the second case, OSI & SAF data were not available and the sea surface temperature, which is held constant throughout the simulation, is interpolated onto the RAMS grid form the ECMWF analysis at 12:00 UTC on 14 October 2012.

3.1 Case of 20 October 2011

The synoptic environment that characterized the storm is shortly discussed. The case study can be classified as a cyclone developing on the lee of the Alps (Buzzi and Tibaldi, 1978). In particular an upper level trough, whose axis was tilted in the SW–NE direction, moved from England toward central Europe. In this movement the upper level winds crossed the western Alps and generated a low-pressure pattern at the surface in the Gulf of Genoa.

Moist air masses were advected at lower tropospheric levels from the Tyrrhenian Sea toward the Italian mainland. The presence of a low pressure pattern, the interaction between the moist air masses with the orographic features of Italy, and the presence of the sea-land contrast triggered convection.

These characteristics of the storm are well shown in Fig. 2, which also suggests the importance of two mesoscale ingredients: (a) the presence of a warm pattern of sea water in the central Tyrrhenian Sea; (b) the convergence of air masses over the Tyrrhenian sea in front of Lazio. Both these features have the potential to strengthen the convection, the former by injecting water vapour into the overlaying atmosphere, the second by triggering convection along the convergence line.

The potential for the development of thunderstorms can be assessed by the K index (KI, Sturtevant, 1995; Yair et al., 2010). It is given by:

$$\mathrm{KI} = (T_{850} - T_{500}) + T_{\mathrm{d}850} - (T_{700} - T_{\mathrm{d}700}) \qquad (7)$$

The KI accounts for the lapse rate (given by the difference between the temperature at 850 hPa, T_{850}, and 500 hPa, T_{500}), for the lower troposphere moisture content (dew point temperature at 850 hPa, $T_{\mathrm{d}850}$), and for the depth of the moisture level (estimated by the

NHESSD
2, 3351–3395, 2014

Simulating lightning into the RAMS model

S. Federico et al.

difference between the temperature at 700 hPa, T_{700}, and the dew point temperature at the same level, T_{d700}). The thunderstorms potential for different values of the KI are as follows (Yair et al., 2010): 0 % for $0 \le KI \le 15$; 20 % or unlikely for $18 \le KI \le 19$; 35 % or isolated thunderstorms for $20 \le KI \le 25$; 50 % or scattered thunderstorm for $26 \le KI \le 29$; 85 % or potential of numerous thunderstorms for $30 \le KI \le 35$; 100 % chance of thunderstorms for $KI > 36$.

Figure 3 shows the value of the KI derived from the ECMWF operational analysis at 00:00 UTC on 20 October. A wide area over Lazio has KI values larger than 29, showing the potential for numerous thunderstorms occurrence.

Figure 4a shows the lightning density recorded by the LINET for the 20 October 2011. The total number of flashes is 16 231 over the whole domain for the whole day, showing an intense electrical activity (the peak is 1521 flashes h^{-1} over the domain). The lightning activity is mainly confined to the West of the Apennines and over the Tyrrhenian Sea, with the largest fraction of flashes occurring between the Apennines and the Sea.

Figure 4b shows the lightning density simulated by applying the methodology described in Sect. 2. The total number of simulated flashes is 18 631 with an overestimation (15 %) of the observed flashes. From the comparison of Fig. 4a and b it is apparent that the model well represents the event because most of the convection occurs and is simulated between the Apennines and the Tyrrhenian Sea with few convective cells located in the northern part of the domain. There is a considerable convection observed and simulated over the sea, even if the model has the tendency to underestimate the area of flashes occurrence. This is also evident to the east of the Apennines, where the simulated lightning activity is less than that observed. There are differences (of the order of few tens of kilometres) in the simulated position of the most intense convective cells, nevertheless the model is able to represent well both the intensity and the position of the lightning activity over Lazio.

To better understand how the lightning scheme works, Fig. 5 shows the vertical distribution of the graupel and ice cells and of the vertical velocity simulated along the 41.70° N latitude cross-section. The vertical cross section is at 08:00 UTC, when the

NHESSD
2, 3351–3395, 2014

simulated convection is at its maximum (see below). There are two graupel cells centred around 12.5 and 13.5° E. Those cells are topped by an ice cell and are producing flashes. Within those cells there are two maxima of the vertical velocity forced by the convection: the first ($\approx 10\,\mathrm{m\,s^{-1}}$; 12.5° E – 5500 m) inside the main convective cell, the second ($\approx 3.0\,\mathrm{m\,s^{-1}}$; 13.5° E – 3500 m) in the smaller one.

Figure 6 shows the hourly distribution of the lightning. The comparison between the LINET and RAMS shows that the model is able to simulate quite well also the evolution over time of the event. In particular, the maximum flash number in one hour is overestimated by the model (1887 flashes simulated in one hour compared to 1521 observed) but occurs at the same time (08:00 UTC) as in the observations. There is, however, a delay of the most intense phase of the event because the simulation shows a maximum electrical activity between 08:00 and 10:00 UTC, while the observations show it between 07:00 and 08:00 UTC. It is worth noting that the comparison shown in this section between simulated and observed lighting activity is an immediate and powerful tool to assess the model ability to reproduce the intensity and the evolution of the convection.

3.2 Case of 15 October 2012

The synoptic environment in which this storm developed is somewhat similar to that of 20 October 2011. An upper level trough approached the Mediterranean Basin from NW Europe and interacted with western Alps. Air masses crossed the western Alps, generating a cyclone on the lee of the Alps (Buzzi and Tibaldi, 1978). This situation is well depicted in Fig. 7, which shows a low pressure on the lee of the Alps (e.g. the 1005 hPa isobar) and a cut-off at 500 hPa. The cyclonic pattern of surface winds advected moist air masses from the Tyrrhenian Sea toward the Italian western coasts, developing convection.

The main difference of this storm compared to the 20 October 2011 case study is that the synoptic-scale system moved rapidly to the east and the convection crossed

NHESSD
2, 3351–3395, 2014

Lazio from north to south in few hours. The geopotential cut-off at 500 hPa, for example, was centred over NE Italy at 06:00 UTC on 16 October 2012 (not shown).

Figure 8 shows the KI derived from the ECMWF operational analysis at 18:00 UTC on 15 October 2012. Values larger than 29 are shown in the northern part (> 42.50° N) and in the southern part (< 41.50° N) of Lazio, with a less chance for thunderstorms in the central part of the region.

Figure 9a shows the lightning density observed by the LINET network on 15 October 2012. The total number of flashes is 4820 and occurred mainly in the late afternoon and evening, with a peak of 1319 flashes h^{-1}. From Fig. 9a it is apparent that there is a considerable lightning activity over the Tyrrhenian Sea, clustered in two main bands of flashes oriented in the southwest-northeast direction, and over the land surface between the Apennines and the sea. However, the comparison of the lightning density registered for the whole day for this and the previous case study (Figs. 5a and 9a), shows that the convection was less intense for 15 October 2012 compared to 20 October 2011.

Figure 9b shows the lightning density simulated using the methodology presented in this paper. The total number of flashes over the domain and for the whole day is 6554 and the model overestimates by 35 % the observed occurrence for this case. Nevertheless, it should be noticed that the model is able to reproduce the less intense lightning activity of this case study compared to the 20 October 2011.

From Fig. 9 it is apparent that the model's representation of the 15 October 2012 event is worse compared to the 20 October 2011; there are two main points to consider: (a) the lightning activity between the Apennines and the Tyrrhenian Sea is simulated by the model, nevertheless its pattern is shifted to the south-east (O(100 km)) with respect to the observations; (b) the lightning activity over the Tyrrhenian Sea is not well reproduced because the model misses the northernmost band of flashes, and the southernmost band is modelled to the South-East of the observed band.

To gain a better understanding of the model performance for this case study, Fig. 10 shows the hourly distribution of registered and simulated flashes on 15 October 2012 over the domain of Fig. 9. The LINET shows the development of convection in the early hours of the day, which is missed by the model. However, the most intense convective activity occurred, by far, in the late afternoon and evening. RAMS correctly depicts the most intense phase of the convection starting in the afternoon, and the maximum lightning rate occurred at 17:00 UTC. Nevertheless the maximum lightning rate is underestimated by the model (1012 flashes per hour simulated over the whole domain of Fig. 9 compared to 1319 flashes per hour observed), and the event duration is longer compared to the observations. For example, the model is producing a sizeable amount of flashes (497 flashes per hour over the whole domain of Fig. 9) still at 21:00 UTC, when the observations show that the lightning activity is very low (28 flashes per hour over the same domain) and it is ending.

To show that the delay in the lightning activity is caused by errors in the meteorological model and are not tied to the lightning scheme itself, Fig. 11 shows the model vertical cross section of graupel, ice and vertical velocity at 21:00 UTC and along the 41.20° N latitude. There are three graupel cells topped by an ice cell, showing that the convection is well active in the model simulation. The graupel cells are producing lightning. The westernmost graupel cell (13.2° E) is above the sea, while the two easternmost (14° E) cells are above the land surface. The vertical velocity shows several local maxima/minima forced by the convection, but, as expected, their values are lower than those simulated for the 15 October 2011 case study (Fig. 5).

The persistence of the simulated lightning activity long after the end of the actual activity is the main cause of the modelled lightning number overestimation for this case study. It can be caused by several factors, which are not easy to separate and quantify due to their interaction. Among others, the extended duration of the lightning activity, particularly over the sea, might indicate a problem with the sedimentation scheme of RAMS, causing the graupel to remain aloft for a long time instead of falling down to the surface.

NHESSD
2, 3351–3395, 2014

The above results show also that errors in the simulated microphysical fields are directly transferred to the lightning scheme and to the simulated lightning distribution. This is one of the drawbacks of using the simple lightning scheme adopted in this study.

The results for this case study show that the lightning simulation may be affected by a spatial displacement error of the order of tens of kilometres and by a temporal error of few hours. It is recognized that these errors are significant from a practical point of view and limit the application of the lightning forecast at finer spatial and temporal scales, nevertheless they are typical of the current state-of-the-art cold started cloud resolving models, as reported in several papers on the subject (McCaul et al., 2009; Yair et al., 2010; DHS2) and as confirmed by the analysis of the objective scores for the other case studies considered in this paper (Sect. 3.3). These errors can be reduced by using data assimilation techniques and, particularly, by the assimilation of lightning data (Fierro et al., 2013).

It is finally stressed that the displacement in time and space of the simulated lightning activity is an effective diagnostic tool to evidence problems in the forecast of the convection. This shows the importance of the use of computationally efficient lightning schemes, such as the one described in this paper, in forecast models.

3.3 Statistical scores

To cast the model performance in an objective way, statistical verification was performed by calculating the hits (a), false alarms (b), and misses (c) for the case studies of 20 October 2011 and 15 October 2012. Starting from those statistics, the probability of detection (POD), false alarm rate (FAR), the bias, and the threat score (TS, also known as Critical Success Index) were computed (Price et al., 2011; Lynn et al., 2012):

$$\mathrm{POD} = \frac{a}{a+c}$$

$$\mathrm{FAR} = \frac{b}{a+b}$$

$$\mathrm{Bias} = \frac{a+b}{a+c}$$

$$\mathrm{TS} = \frac{a}{a+b+c}$$

The scores were computed for different grid overlays (35 km, 25 km, 12.5 km and 5 km grid element size) superimposed to the RAMS grid at 2.5 km resolution for the day considered (24 h), 20 October 2011 and 15 October 2012 respectively. The statistics is presented for the subdomain of the second grid shown in Fig. 4 (10.5–14.5° E, 40.5–43.5° N). Two different minimum thresholds of lightning events per grid overlay element are used to compute the scores: ≥ 1 (i.e., a hit is when there is at least 1 simulated lightning event and at least 1 registered lightning event in the same grid overlay element) and ≥ 10 (i.e., a hit is when there are at least 10 simulated lightning events and at least 10 registered lightning events in the same grid overlay element). Hereafter, these thresholds are referred to as MLT1 (minimum lightning threshold ≥ 1) and MLT10 (minimum lightning threshold ≥ 10).

Results are shown in Fig. 12. The performance decreases for smaller grid element sizes, showing the difficulty to simulate correctly the exact location of the lightning activity at finer scales. In particular, for MLT1, the POD for the 20 October 2011 (15 October 2012) decreases from 0.77 (0.87) for the 35 km overlay to 0.58 (0.42) for the 5 km overlay, while the FAR increases from 0.16 (0.11) for the 35 km overlay to 0.18 (0.58) for the 5 km overlay. It is noticed that POD is larger than FAR for all grid overlays on 20 October 2011, while POD is less than FAR for the 5 km overlay on 15 October 2012.

The results for the MLT10 are worse. On 20 October 2011 the POD is larger than FAR for the 35 km, 25 km and 12.5 km overlays (not for the 5 km overlay), while, on 15

NHESSD

2, 3351–3395, 2014

Simulating lightning into the RAMS model

S. Federico et al.

October 2012, POD is larger than FAR only for the 35 km and 25 km overlays (not for the 12.5 km and 5 km overlays). These results show the difficulty of correctly predicting the exact location of intense convective cells. Similar results were found by Lynn et al. (2012) considering an event in the Central US (Tuscaloosa, 27 April 2012). They considered the 36, 12 and 4 km grid overlay sizes superimposed to the 4 km WRF grid (Fig. 8 of Lynn et al., 2012) and found a decrease of the performance for smaller grid sizes and for higher minimum lightning per grid element thresholds. In particular, for the 4 km overlay, the POD was larger than FAR for MLT1, while POD was less than FAR for MLT10.

The statistics of Fig. 12 show, as suggested from the results presented in the previous two sections, that the model performance was better for the 20 October 2011 compared to the 15 October 2012.

To make the results of this paper statistically more robust, four additional case studies occurred in fall 2012 are considered. The cases refer to moderate-high lightning activity over Lazio (6666 to 14 357 lightning per day, Table 2) and occurred on 3 September, 30 September, 11 November, and 28 November 2012.

RAMS simulations for these cases were performed using the same grid configuration (Table 1, Fig. 1) as that used for the 20 October 2011 and 15 October 2012 case studies, using the ECMWF operational analysis (0.25° horizontal resolution) as initial and boundary conditions. Simulations last 36 h and were initialized at 12:00 UTC on the day preceding the case study (12 h spin-up time). Sea surface temperature was interpolated onto the RAMS grids from ECMWF analyses.

The scores for the 25 km, 12.5 km and 5 km grid overlays, for the whole day of each of the six simulations and for MLT1 and MLT10 are shown in Table 2. Considering the 25 km overlay, it is noticed that POD is always larger than FAR for both lightning thresholds considered. Considering MLT1, the Bias ranges from 0.84 (11 November 2011) to 1.03 (30 September 2012). TS ranges from 0.61 (20 October 2011) to 0.89 (28 November 2012). The performance decreases for MLT10. The threat score ranges between

0.45 (3 September 2012) and 0.76 (28 November 2012). The Bias ranges between 0.80 (11 November 2012) and 1.25 (30 September 2012).

For the 12.5 km overlay, the performance is worse compared to the 25 km overlay for both lightning thresholds. Nevertheless, it is noticed that for MLT1 POD is larger than FAR for all case studies, showing a good performance. The Bias ranges from 0.78 (11 November 2012) to 1.08 (30 September 2012), while TS ranges from 0.54 (15 October 2012) to 0.76 (28 November 2012). For MLT10 POD is larger than FAR for three cases only, namely 20 October 2011, and 11 and 28 November 2012, showing less satisfactory results. This is confirmed by the values of TS, which are lower than 0.5 for all case studies except on 11 November 2012, where TS is 0.53, and on 20 October 2011, where TS is 0.60. The Bias ranges from 0.65 (28 November 2012) to 1.23 (15 October 2012).

For the 5 km overlay the results are worse than for the two larger overlays. However, for the MLT1 the POD is larger than FAR for three cases studies (20 October 2011, 11 and 28 November 2012). The Bias ranges from 0.69 (28 November 2012) to 1.16 (30 September 2012), while the TS ranges from 0.27 (15 October 2012) to 0.52 (20 October 2011 and 11 November 2012). For the MLT10 the POD is always lower than FAR. The BIAS ranges from 0.94 (28 November 2012) to 1.97 (15 October 2012), while the value of TS is zero or near zero for three case studies (3 and 30 September 2012, and 15 October 2012).

In summary, the statistics of Table 2 shows a decrease of the performance of the lightning simulation at finer horizontal scales and for the higher minimum thresholds of lightning events per grid element. This result confirms the findings of other authors and shows the difficulty to correctly simulate the exact position and intensity of the convective cells. It is also stressed that the results of Table 2 quantify objectively that the model had a better performance on 20 October 2011 than on 15 October 2012, and that the cases study presented in detail in the previous two sections span a wide range of model performance as well as of lightning number recorded over the area of study.

NHESSD

2, 3351–3395, 2014

It is interesting to consider the performance of the lightning scheme for other lightning thresholds. Figure 13 shows the number of grid elements where the simulated lightning number and that recorded by LINET are higher than the MLT value, for different thresholds and for the 5 km overlay. The distributions are obtained by summing over all cases. For the lowest threshold MLT1 (≥ 1 lightning per grid element), our method underestimates the lightning distribution, which is less spatially extended compared to the observations. This determines a Bias lower than 1.

For the larger thresholds (≥ 10 lightning per grid element threshold), our method overestimates the observed distribution and it has a larger spatial extension compared to the observations. This determines a Bias larger than 1. This behaviour is also shown by the results of Table 2.

The same behaviour is obtained for the other grid overlays (not shown) showing a general tendency of the model.

For Fig. 13, however, it should be considered that:

a. It is obtained by suming over all cases and exceptions to the above results can occur for particular cases.

b. Despite the modelled and observed distributions may show similar values as, for example, for MLT5, the spatial pattern of these distributions can differ, determining low values of TS and poor prediction. The results for the cases considered in this paper show a decrease of the TS with increasing thresholds and decreasing grid overlay size.

4 Conclusions

This study shows the application of a new methodology to simulate lightning activity and produce lightning occurrence maps implemented into the RAMS model. The methodology has been applied to six case studies occurred over the Lazio Region, in central Italy. Two of them were presented in detail. The first, occurred on 20 October 2011, was well represented by the model and was characterized by an intense lightning activity; the second, occurred on 15 October 2012, was characterized by moderate lightning activity and was less adequately represented by the model. The number of flashes simulated (observed) over Lazio is 18 631 (16 231) for the first case and 6554 (4820) for the second case. The results show that the model correctly simulates the larger number of flashes that characterized the first event compared to the second.

The analysis of the two cases shows that, particularly on 15 October 2012, there are errors in the timing (O(3 h)) and in the position (O(100 km)) of the convection, which are reflected in the simulated spatial and temporal distribution of the flashes.

It is evident that the errors in the simulated convection (timing errors, position error, and intensity of convention) are directly transferred to the simulated lightning field. This is the main drawback of the method implemented in this work and in many others reported in the literature. In addition to RAMS deficiencies in the parameterization of the physical processes, initial and dynamic boundary conditions could also play a role and the analysis of the meteorological parameters at the mesoscale and rapid updated forecasting cycles would very likely mitigate these weaknesses.

There are drawbacks in the lightning scheme too. Our method is independent of the polarity, and in particular does not consider positive cloud-to-ground flashes, which can account to 5–10 % of total cloud-to-ground flashes (Altaraz et al., 2003). Moreover it does not properly accounts for the characteristics of intra cloud flashes, which are measured by LINET. Recently, Lynn et al. (2012) introduced a scheme using the dynamic and microphysics fields of the cloud resolving model WRF to calculate the electrical potential energy for positive and negative cloud-to-ground and intra cloud flashes. The different kinds of flashes (positive and negative cloud-to-ground and intra cloud) were properly taken into account by considering their specific characteristics (currents, threshold energy for the discharge, etc.).

Another drawback of the lightning scheme is that all the energy accumulated in the plane capacitor is converted to flashes in a single application of the lightning scheme.

NHESSD
2, 3351–3395, 2014

Lynn et al. (2012) showed the importance of the advection of the electric potential energy from one grid-cell to another as a producer of lightning.

Despite these issues, which contributed to cause discrepancy between observed and measured lightning activity, statistical scores show objectively the ability of the methodology implemented in this paper to simulate the daily lightning activity for several spatial scales and for two different minimum thresholds of lightning events (per grid element).

An advantage of using the methodology presented is that it is simple to implement and computationally fast. It takes 5 s of a state of the art desktop computer to elaborate once the lightning scheme for both domains of Fig. 1. This is important for several applications, based on nowcasting and short-term forecasting of the lightning activity, such as ground service planning in airports or in general for outdoor activities where public safety could be affected by lightning. Moreover, our scheme, being based on the ice and mixed phase hydrometeors simulated by RAMS is more physically based compared to the methods using thermodynamic indices, as shown by several studies (Petersen et al., 2005; Katsanos et al., 2007a; Yair et al., 2010).

Besides future studies dedicated specifically to solve some critical issues of our methodology, such as the inclusion of the lightning polarity, there are at least two main directions for future development of the research presented in this paper:

a. The use of lightning data assimilation to improve the forecast in time and space of the convective activity, especially its triggering over the sea.

b. The improvement of the physics and dynamic of the model for better representing the microphysical field and the derived lightning activity.

Finally, the lightning simulation presented in this paper can be exploited in an ensemble system, using a similar approach to that described by Federico et al. (2008), based on the comparison between model pseudo water vapour images and METEOSAT scenes in the water vapour channel. One could use the observed lightning activity, and its evolution in time, to choose the members of the ensemble that have a simulated lightning activity in better agreement with the observations. Since lightning distribution is well correlated to areas with the severe convection, more confidence would be given to those members in forecasting the heavy precipitation, thus providing valuable information to the forecasters.

Acknowledgements. The ECMWF and Aeronautica Militare – CNMCA are acknowledged for the access to the MARS database. Part of the computations of this paper was performed on the ECMWF supercomputing environment through the special project SPITFEDE. LINET data were provided by Nowcast GmbH (https://www.nowcast.de/) within a scientific agreement between H.-D. Betz and the Satellite Meteorological Group of CNR-ISAC in Rome.

References

Altaratz, O., Levin, Z., Yair, Y., and Ziv, B.: Lightning activity over land and sea on the eastern coast of the Mediterranean, Mon. Weather Rev., 131, 2060–2070, doi:10.1175/1520-0493, 2003.

Barthe, C., Molinie, G., and Pinty, J.: Description and first results of an explicit electrical scheme in a 3-D cloud resolving model, Atmos. Res., 76, 95–113, 2005.

Betz, H. D., Schmidt, K., Laroche, P., Blanchet, P., Oettinger, W. P., Defer, E., Dziewit, Z., and Konarski, J.: LINET – an international lightning detection network in Europe, Atmos. Res., 91, 564–573, 2009.

Bright, D. R., Wandishin, M. S., Jewell, R. E, and Weiss, S. J.: A physically based parameter for lightning prediction and its calibration in ensemble forecasts, Preprints, 22nd Conf. on Severe Local Storms, Hyannis, MA, Amer. Meteor. Soc., 4.3, available at: http://ams.confex.com/ams/pdfpapers/84173.pdf, 2004.

Buzzi, A. and Tibaldi, S.: Cyclogenesis on the lee of the Alps: a case study, Q. J. Roy. Meteor. Soc., 104, 271–287, 1978.

Cecil, D. J., Goodman, S. J, Boccippio, D. J., Zipser, E. J., and Nesbitt, S. W.: Three years of TRMM precipitation features, Part I: Radar, radiometric, and lightning characteristics, Mon. Weather Rev., 133, 543–566, 2005.

Chen, C. and Cotton, W. R.: A one-dimensional simulation of the stratocumulus-capped mixed layer, Bound.-Lay. Meteorol., 25, 289–321, 1983.

Cotton, W. R., Pielke Sr., R. A., Walko, R. L., Liston, G. E., Tremback, C. J., Jiang, H., McAnelly, R. L., Harrington, J. Y., Nicholls, M. E., Carrio, C. G., and McFadden, J. P.: RAMS 2001: current status and future directions, Meteorol. Atmos. Phys., 82, 5–29, 2003.

Curran, E. B., Holle, R. L., and Lopez, R. E.: Lightning casualties and damages in the United States from 1959 to 1994, J. Climate, 13, 3448–3464, 2000.

Dahl, J. M. L., Holler, H., and Schumann, U.: Modeling the flash rate of thunderstorms, Part I: Implementation, Mon. Weather Rev., 139, 3093–3111, 2011a.

Dahl, J. M. L., Holler, H., and Schumann, U.: Modeling the flash rate of thunderstorms, Part II: Implementation, Mon. Weather Rev., 139, 3112–3124, 2011b.

Defer, E., Lagouvardos, K., and Kotroni, V.: Lightning activity in the eastern Mediterranean region, J. Geophys. Res., 110, D24210, doi:10.1029/2004JD005710, 2005.

Deierling, W. and Petersen, W. A.: Total lightning activity as an indicator of updraft characteristics, J. Geophys. Res., 113, D16210, doi:10.1029/2007JD009598, 2008a.

Deierling, W., Petersen, W. A., Latham, J., Ellis, S., and Christian, H.: The relationship between lightning activity and ice fluxes in thunderstorms, J. Geophys. Res., 113, D15210, doi:10.1029/2007JD009700, 2008b.

Federico, S.: Verification of surface minimum, mean, and maximum temperature forecasts in Calabria for summer 2008, Nat. Hazards Earth Syst. Sci., 11, 487–500, doi:10.5194/nhess-11-487-2011, 2011.

Federico, S., Bellecci, C., and Walko, R. L.: A LEPS approach to the predictability of intense rain storms in the Central Mediterranean basin, Adv. Geosci., 16, 89–95, doi:10.5194/adgeo-16-89-2008, 2008.

Fierro, A. O., Gao, J., Ziegler, C. L., Mansell, E. R., Macgorman, D. R., and Dembek, S. R.: Evaluation of a cloud scale lightning data assimilation technique and a 3DVAR method for the analysis and short-term forecast of the 29 June 2012 derecho event, Mon. Weather Rev., 142, 183–202, doi:10.1175/MWR-D-13-00142.1, 2013.

Formenton, M., Panegrossi, G., Casella, D., Dietrich, S., Mugnai, A., Sanó, P., Di Paola, F., Betz, H.-D., Price, C., and Yair, Y.: Using a cloud electrification model to study relationships between lightning activity and cloud microphysical structure, Nat. Hazards Earth Syst. Sci., 13, 1085–1104, doi:10.5194/nhess-13-1085-2013, 2013.

Goodman, S. J., Buechler, D., and McCaul, E.: Lightning, in: Our Changing Planet: the View from Space, edited by: King, M., Parkinson, C., Partington, K., and Williams, R., Cambridge University Press, 44–52, 2007.

NHESSD
2, 3351–3395, 2014

Grewe, V.: Impact of Lightning on Air Chemistry and Climate, Lightning: Principles, Instruments and Applications, edited by: Betz, H.-D., Schumann, U., and Laroche, P., Springer, 537–549, 2009.
Gungle, B. and Krider, E. P.: Cloud-to-ground lightning and surface rainfall in warm-season Florida thunderstorms, J. Geophys. Res., 111, D19203, doi:10.1029/2005JD006802, 2006.
Heymsfield, A. and Kajikawa, M.: An improved approach to calculating terminal velocities of plate-like crystals and graupel, J. Atmos. Sci., 44, 1088–1099, 1987.
Hoshen, J. and Kopelman, R.: Percolation and cluster distribution, I. Cluster multiple labeling technique and critical concentration algorithm, Phys. Rev. B, 14, 3438–3445, 1976.
Katsanos, D., Lagouvardos, K., Kotroni, V., Argiriou, A.: Combined analysis of rainfall and lightning data produced by mesoscale systems in the central and eastern Mediterranean, Atmos. Res., 83, 55–63, doi:10.1016/j.atmosres.2006.01.012, 2007a.
Katsanos, D., Lagouvardos, K., Kotroni, V., Argiriou, A.: Relationship of lightning activity with microwave brightness temperatures and spaceborne radar reflectivity profiles in the central and eastern Mediterranean, J. Appl. Meteorol. Clim., 46, 1901–1912, 2007b.
Kuo, H. L.: Further studies of the parameterization of the influence of cumulus convection on large-scale flow, J. Atmos. Sci., 31, 1232–1240, 1974.
Land, T. L. and Rutledge, S. A.: Relationships between convective storm kinematics, precipitation, and lightning, Mon. Weather Rev., 130, 2492– 2506, doi:10.1175/1520-0493, 2002.
Latham, J., Blyth, A. M., Christian Jr., H. J., Deierling, W., and Gadian, A. M.: Determination of precipitation rates and yields from lightning measurements, J. Hydrol., 288, 13–19, doi:10.1016/j.jhydrol.2003.11.009, 2003.
Lynn, B., Yair, Y., Price, C., Kelman, G., and Clark, A. J.: Predicting cloud-to-ground and intracloud lightning in weather forecast models, Weather Forecast., 27, 1470–1488, doi:10.1175/WAF-D-11-00144.1, 2012.
MacGorman, D., Straka, J., and Ziegler, C.: A lightning parameterization for numerical cloud models, J. Appl. Meteorol., 40, 459–478, 2001.
Mansell, E. R., MacGorman, D., Ziegler, C. L., and Straka, J. M.: Simulated three-dimensional branched lightning in a numerical thunderstorm model, J. Geophys. Res., 107, 4075, doi:10.1029/2000JD000244, 2002.
Mansell, E. R., MacGorman, D., Ziegler, C., and Straka, J. M.: Charge structure and lightning sensitivity in a simulated multicell thunderstorm, J. Geophys. Res., 110, D12101, doi:10.1029/2004JD005287, 2005.

NHESSD
2, 3351–3395, 2014

McCaul Jr., E., Goodman, S. J., LaCasse, K. M., and Cecil, D. J.: Forecasting lightning threat using cloud-resolving model simulations, Weather Forecast., 24, 709–729, 2009.
Molinari, J. and Corsetti, T.: Incorporation of cloud-scale and mesoscale down-drafts into a cumulus parametrization: results of one and three-dimensional integration, Mon. Weather Rev., 113, 485–501, 1985.
OSI & SAF: High Latitude SST product manual, version 1.2, 10/10/2002 Met. no, Oslo (Norway), available at: http://www.osi-saf.org, 2006.
Petersen, W. A, Christian, H. J., and Rutledge, S. A.: TRMM observations of the global relationship between ice water content and lightning, Geophys. Res. Lett, 32, L14819, doi:10.1029/2005GL023236, 2005.
Pielke, R. A.: Mesoscale Meteorological Modeling, Academic Press, San Diego, 676 pp., 2002.
Price, C. and Federmesser, B.: Lightning-rainfall in Mediterranean winter thunderstorms, Geophys. Res. Lett., 33, L07813, doi:10.1029/2005GL024794, 2006.
Price, C. and Rind, D.: A simple lightning parameterization for calculating global lightning distributions, J. Geophys. Res., 97, 9919–9933, 1992.
Price, C., Yair, Y., Mugnai, A., Lagouvardos, K., Llasat, M. C., Michaelides, S., Dayan, U., Dietrich, S., Di Paola, F., Galanti, E., Garrote, L., Harats, N., Katsanos, D., Kohn, M., Kotroni, V., Llasat-Botija, M., Lynn, B., Mediero, L., Morin, E., Nicolaides, K., Rozalis., S., Savvidou, K., and Ziv, B.: Using lightning data to better understand and predict flash floods in the Mediterranean, Surv. Geophys., 32, 733–751, doi:10.1007/ss10712-011-9146-y, 2011.
Saunders, C. P. R.: Charge separation mechanisms in clouds, Space Sci. Rev., 137, 335–353, 2008.
Smagorinsky, J.: General circulation experiments with the primitive equations, Part I, The basic experiment, Mon. Weather Rev., 91, 99–164, 1963.
Solomon, R. and Baker, M.: A one-dimensional lightning parameterization, J. Geophys. Res., 101, D10, 14983–14990, doi:10.1029/96JD00941, 1996.
Solomon, R., Medaglia, C. M., Adamo, C., Dietrich, S., Mugnai, A., and Biader Ceipidor, U.: An explicit microphysics thunderstorm model, Int. J. Model. Simul., 25, 112–118, 2005.
Soula, S., Sauvageot, H., Molinieé, G., Mesnard, F., and Chauzy, S.: The CG lightning activity of a storm causing a flash-flood, Geophys. Res. Lett., 25, 1181–1184, doi:10.1029/98GL00517, 1998.
Stauffer, D. and Aharony, A.: Introduction to percolation theory, Taylor and Francis, London, 181 pp., 1994.

Sturtevant, J. S.: The severe local storm forecasting primes, Weather Scratch Meteorolo. Serv., Florence, Ala., 197 pp., 1995.
Tapia, A., Smith, J. A., and Dixon, M.: Estimation of convective rainfall from lightning observations, J. Appl. Meteorol., 37, 1497–1509, doi:10.1175/1520-0450, 1998.
Walko, R. L., Cotton, W. R., Meyers, M. P., and Harrington, J. Y.: New RAMS cloud microphysics parameterization part I: the single-moment scheme, Atmos. Res., 38, 29–62, 1995.
Walko, R. L., Band, L. E., Baron, J., Kittel, T. G., Lammers, R., Lee, T. J., Ojima, D., Pielke Sr., R. A., Taylor, C., Tague, C., Tremback, C. J., and Vidale, P. L.: Coupled Atmosphere-Biosphere-Hydrology Models for environmental prediction, J. Appl. Meteorol., 39, 931–944, 2000.
Wong, J., Barth, M. C., and Noone, D.: Evaluating a lightning parameterization based on cloud-top height for mesoscale numerical model simulations, Geosci. Model Dev., 6, 429–443, doi:10.5194/gmd-6-429-2013, 2013.
Yoshida, S., Morimoto, T., Ushio, T., and Kawasaki, Z.: A fifth- power relationship for lightning activity from tropical rainfall measuring mission satellite observations, J. Geophys. Res., 114, D09104, doi:10.1029/2008JD010370, 2009.
Yair, Y., Lynn, B., Price, C., Kotroni, V., Lagouvardos, K., Morin, E., Mugnai, A., and Llasat, M. C.: Predicting lightning density in Mediterranean storms based on the WRF model dynamic and microphysical fields, J. Geophys. Res., 125, D04205, doi:10.1029/2008JD010868, 2010.
Zhou, Y., Qie, X., and Soula, S.: A study of the relationship between cloud-to-ground lightning and precipitation in the convective weather system in China, Ann. Geophys., 20, 107–113, doi:10.5194/angeo-20-107-2002, 2002.

NHESSD
2, 3351–3395, 2014

Table 1. RAMS grid-setting. NNXP, NNYP and NNYZ are the number of grid points in the west-east, north-south, and vertical directions. Lx (km), Ly (km), Lz (m) are the domain extension in the west-east, north-south, and vertical directions. DX (km) and DY (km) are the horizontal grid resolutions in the west-east and north-south directions. CENTLON and CENTLAT are the geographical coordinates of the grid centres.

	Domain 1	Domain 2
NNXP	300	182
NNYP	300	182
NNZP	35	35
Lx	3000 km	455 km
Ly	3000 km	455 km
Lz	21 800 m	21 800 m
DX	10 km	2.5 km
DY	10 km	2.5 km
CENTLAT (°)	42.0	42.0
CENTLON (°)	12.5	12.5

NHESSD
2, 3351–3395, 2014

Simulating lightning into the RAMS model

S. Federico et al.

Table 2. Skill score statistics of the six case studies. Date of forecast and number of flashes observed (LINET) and simulated (RAMS) for each case study are shown in the first column. POD, FAR, Bias, and TS are given for the MLT1 and MLT10 (in parentheses) for the 25 km, 12.5 km and 5 km overlays superimposed to the 2.5 km RAMS grid. The area considered for the statistics is the area shown in Fig. 4 (10.5–14.5° E, 40.5–43.5° N).

	25 km overlay				12.5 km overlay				5 km overlay			
Case study	POD	FAR	Bias	TS	POD	FAR	Bias	TS	POD	FAR	Bias	TS
20111020 LINET: 16231 RAMS: 18631	0.73 (0.76)	0.21 (0.17)	0.92 (0.91)	0.61 (0.66)	0.66 (0.68)	0.18 (0.17)	0.80 (0.82)	0.58 (0.60)	0.58 (0.46)	0.18 (0.51)	0.71 (0.95)	0.52 (0.31)
20120903 LINET: 6666 RAMS: 6496	0.85 (0.58)	0.09 (0.33)	0.93 (0.88)	0.78 (0.45)	0.68 (0.43)	0.25 (0.55)	0.91 (0.97)	0.55 (0.28)	0.43 (0.18)	0.56 (0.84)	0.99 (1.07)	0.28 (0.01)
20120930 LINET: 7073 RAMS: 7635	0.90 (0.85)	0.13 (0.32)	1.03 (1.25)	0.79 (0.61)	0.79 (0.46)	0.27 (0.62)	1.08 (1.20)	0.61 (0.26)	0.53 (0.05)	0.54 (0.96)	1.16 (1.01)	0.33 (0.02)
20121015 LINET: 4820 RAMS: 6554	0.80 (0.68)	0.20 (0.38)	1.00 (1.09)	0.66 (0.48)	0.70 (0.40)	0.29 (0.67)	0.99 (1.23)	0.54 (0.22)	0.42 (0.01)	0.58 (0.99)	1.01 (1.97)	0.27 (0.03)
20121111 LINET: 9030 RAMS: 12308	0.79 (0.76)	0.05 (0.05)	0.84 (0.80)	0.76 (0.73)	0.73 (0.65)	0.06 (0.25)	0.78 (0.87)	0.69 (0.53)	0.62 (0.31)	0.24 (0.80)	0.81 (1.53)	0.52 (0.14)
20121128 LINET: 14357 RAMS: 13842	0.90 (0.79)	0.02 (0.06)	0.92 (0.84)	0.89 (0.76)	0.80 (0.46)	0.06 (0.29)	0.85 (0.65)	0.76 (0.39)	0.52 (0.15)	0.25 (0.83)	0.69 (0.94)	0.45 (0.09)

NHESSD
2, 3351–3395, 2014

NHESSD
2, 3351–3395, 2014

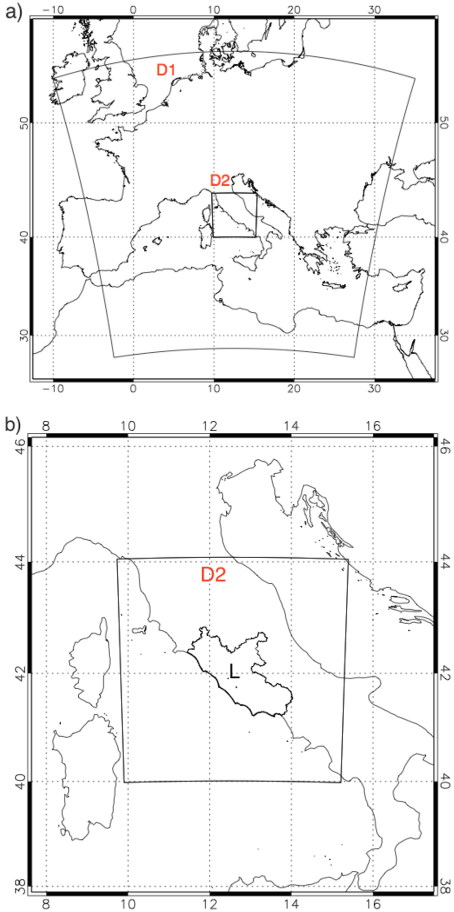

Fig. 1. (a) Domains used in this paper; **(b)** The Lazio Region (L) in the second domain.

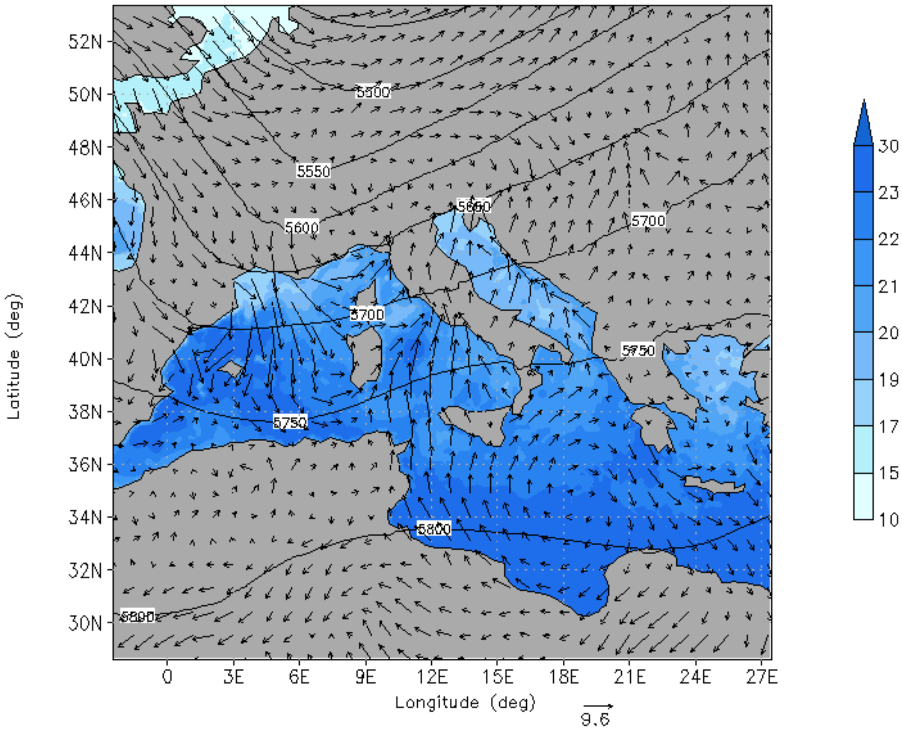

Fig. 2. The 20 October 2011 case study. Geopotential height at 500 hPa (m, black contours) sea surface temperature (°C, filled contours), and surface winds ($m\,s^{-1}$, vectors plotted every ten grid points). The upper level trough, tilted in the SW–NE direction, and the cyclonic wind at the surface on the lee of the western Alps are well evident. The graph is on 20 October at 00:00 UTC and is derived from the RAMS output.

NHESSD
2, 3351–3395, 2014

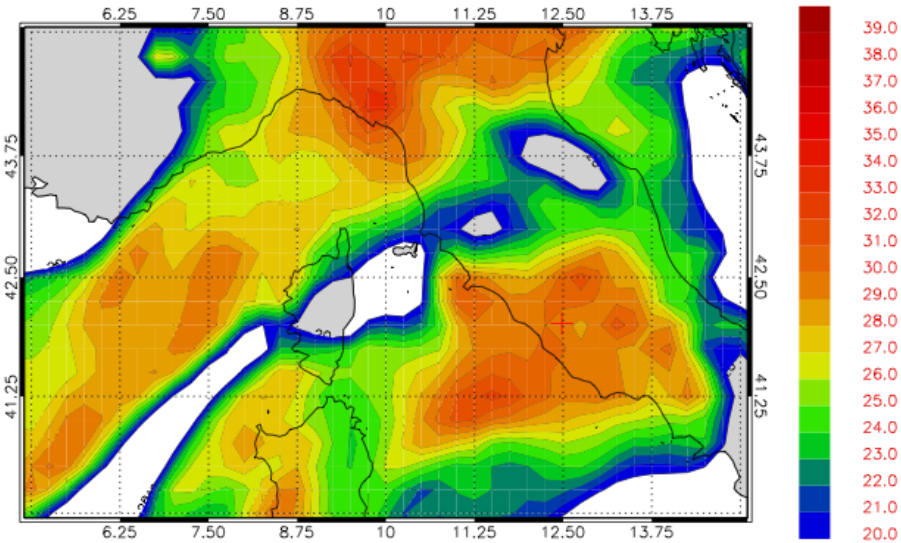

Fig. 3. KI at the 00:00 UTC on 20 October 2011.

NHESSD
2, 3351–3395, 2014
Simulating lightning into the RAMS model
S. Federico et al.

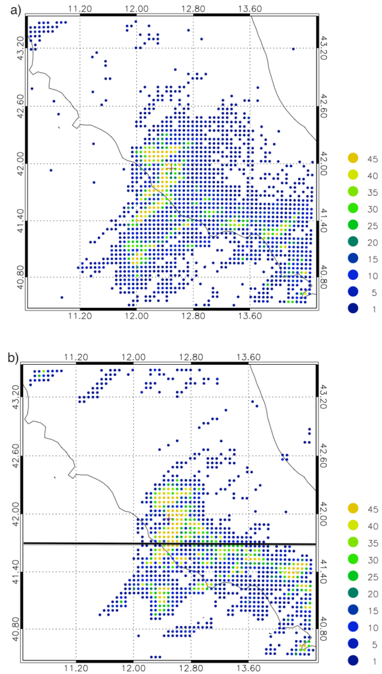

Fig. 4. (a) Flash density (number of flashes per 25 km^2 and accumulated over the whole day) measured by the LINET network on 20 October 2011; **(b)** flashes density (number of flashes per 25 km^2 and accumulated over the whole day) simulated by applying the DHS method on 20 October 2011. To obtain the flash densities of Fig. 4, observed flashes for the whole day have been remapped onto a 5 km × 5 km grid, and the modelled flash density (ρ_{fl}) has been integrated over the same grid and for the whole day. Only grid-boxes having at least one flash are shown. The black solid line in Fig. 4b shows the latitude of the cross section of Fig. 5.

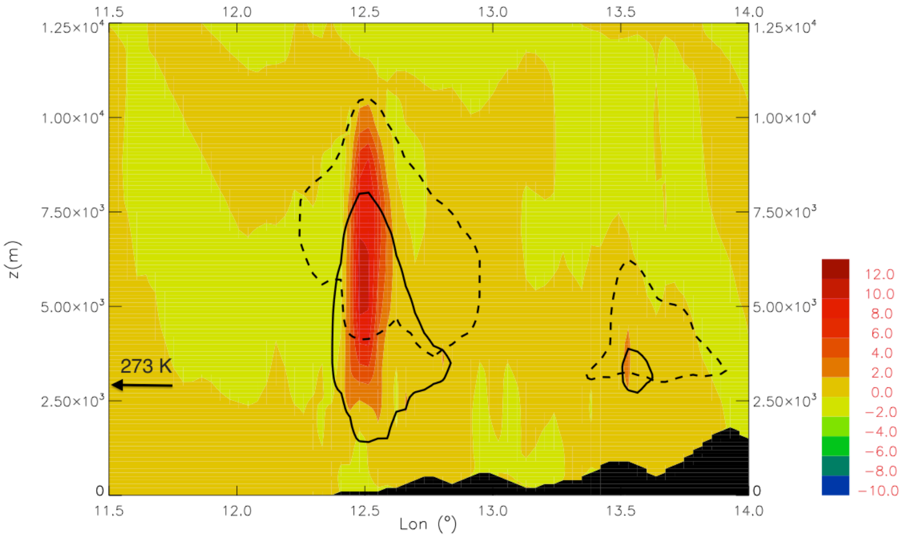

Fig. 5. Longitude-height cross section (latitude 41.70° N) at 08:00 UTC on 20 October 2011. Solid contours show areas where graupel density is larger than 0.1 $\mathrm{g\,m^{-3}}$ (graupel cell); dashed contours shows areas where ice density is larger than 0.1 $\mathrm{g\,m^{-3}}$ (ice cell). Color filled contours indicate the vertical velocity ($\mathrm{m\,s^{-1}}$). The height of the 273 K isotherm is roughly indicated. The black mask at the bottom of the figure shows the RAMS orography.

NHESSD
2, 3351–3395, 2014

Simulating lightning into the RAMS model

S. Federico et al.

Title Page
Abstract Introduction
Conclusions References
Tables Figures
◀I ▶I
◀ ▶
Back Close
Full Screen / Esc
Printer-friendly Version
Interactive Discussion

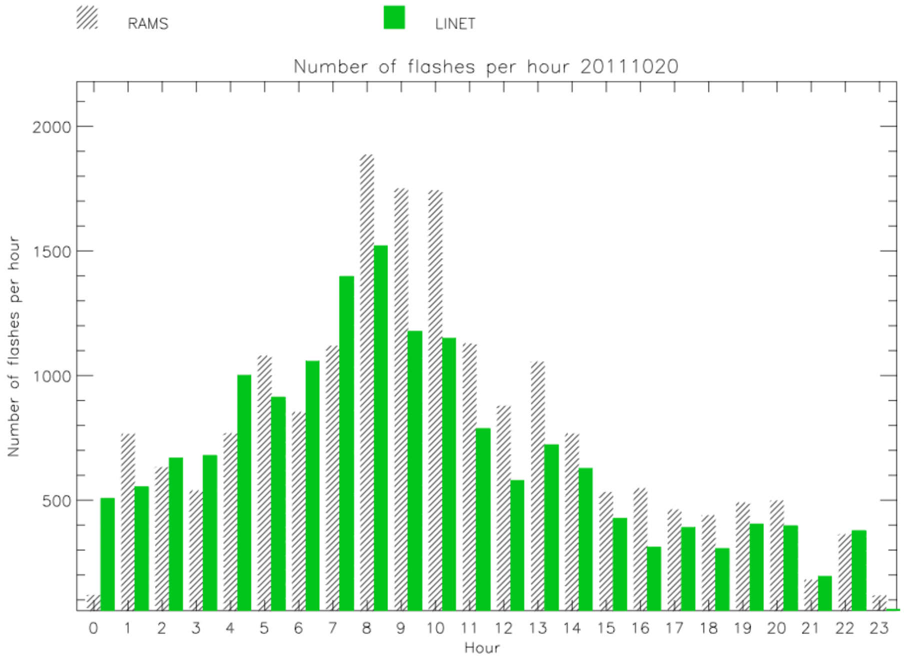

Fig. 6. Lightning number (h^{-1}) recorded (LINET) and simulated (RAMS) on 20 October 2011 over the domain of Fig. 4.

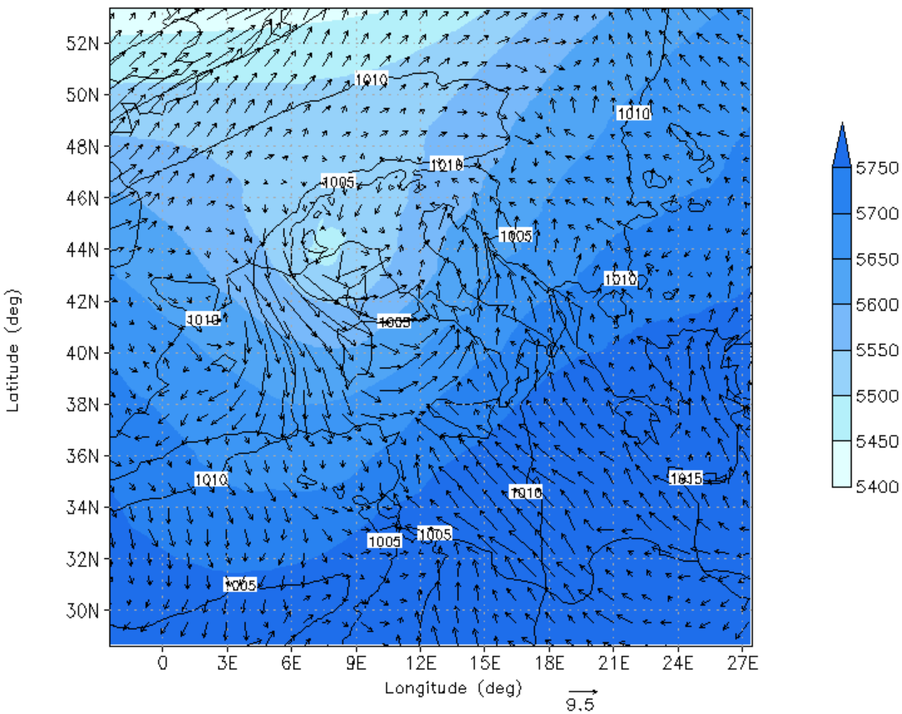

Fig. 7. The synoptic environment of the 15 October 2012 case study. Geopotential height at 500 hPa (m, filled contours); sea level pressure (hPa, black contours); surface wind ($m\,s^{-1}$, vectors plotted every ten grid points). The Figure is on 15 October 2012 at 18:00 UTC and is derived from the RAMS output.

NHESSD

2, 3351–3395, 2014

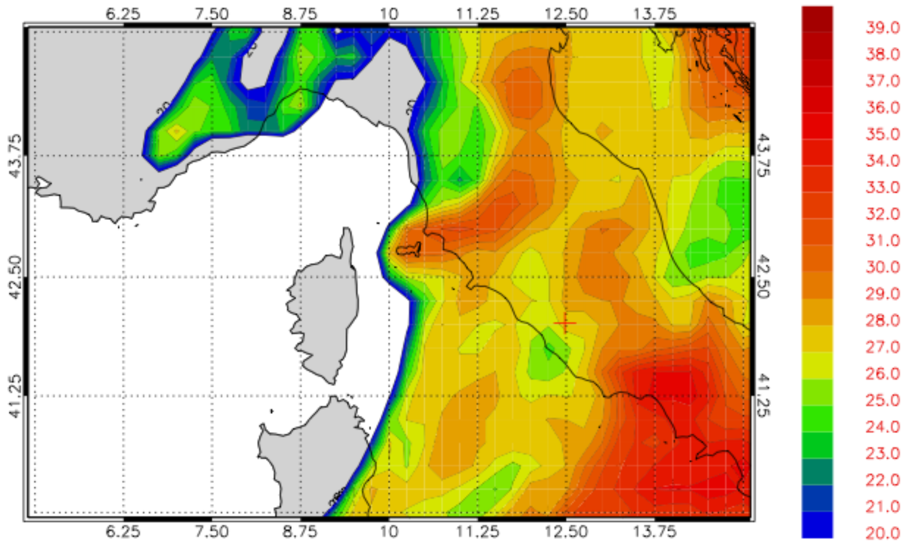

Fig. 8. KI at the 18:00 UTC on 15 October 2012.

NHESSD
2, 3351–3395, 2014

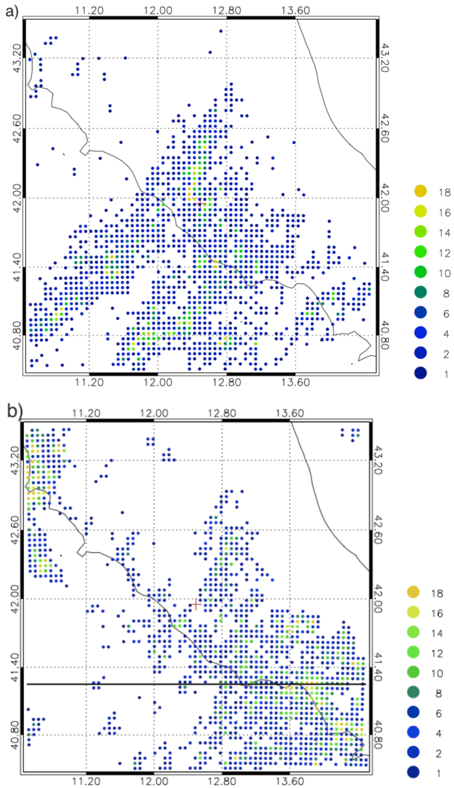

Fig. 9. (a) flash density (number of flashes per 25 km^2 and cumulated over the whole day) measured by the LINET network on 15 October 2012; **(b)** flash density (number of flashes per 25 km^2 and cumulated for the whole day) simulated by applying the DHS method on 15 October 2012. To obtain the densities of Fig. 9, observed flashes for the whole day have been remapped onto a 5 km × 5 km grid, and the modelled flash density (ρ_{fl}) has been integrated over the same grid and for the whole day. Only grid-boxes having at least one flash are shown. The black solid line in **(b)** shows the latitude of the cross section of Fig. 11.

NHESSD
2, 3351–3395, 2014

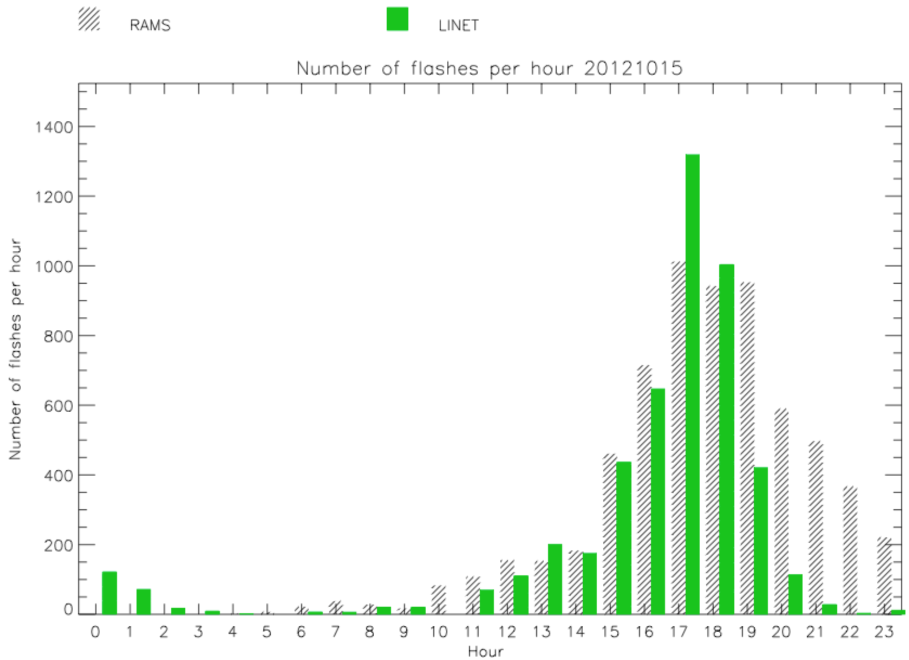

Fig. 10. Lightning number $(h)^{-1}$ recorded (LINET) and simulated (RAMS) on 15 October 2012 over the domain of Fig. 9.

NHESSD
2, 3351–3395, 2014

Simulating lightning into the RAMS model

S. Federico et al.

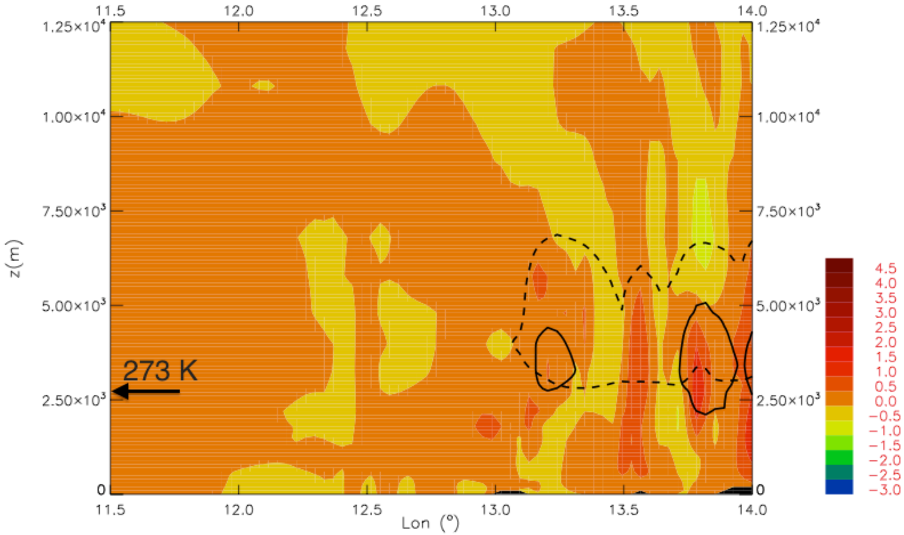

Fig. 11. Longitude-height section (latitude 41.20° N) at 21:00 UTC on 15 October 2012. Solid contours show areas where graupel density is larger than 0.1 $g\,m^{-3}$ (graupel cell); dashed contours shows areas where ice density is larger than 0.1 $g\,m^{-3}$ (ice cell). Color filled contours indicate the vertical velocity ($m\,s^{-1}$). The height of the 273 K isotherm is roughly indicated. The black mask at the bottom of the figure shows the RAMS orography.

NHESSD
2, 3351–3395, 2014

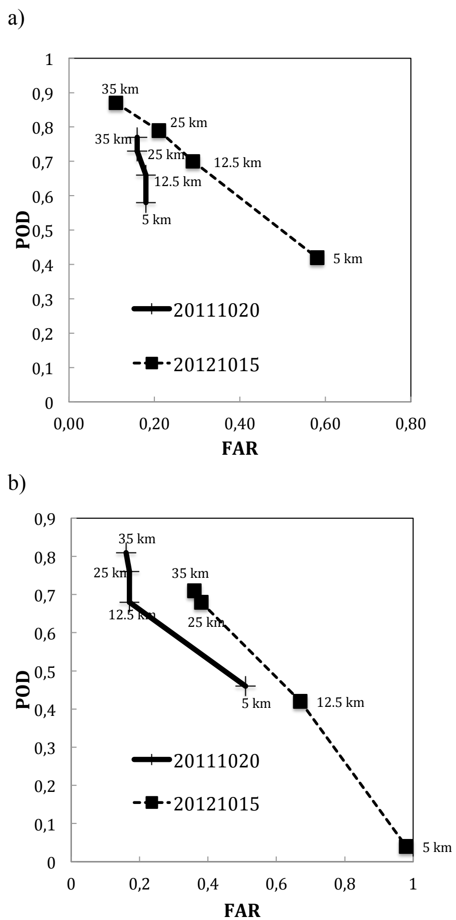

Fig. 12. POD (vertical axis) plotted against FAR (horizontal axis) for the 20 October 2011 (solid line) and the 15 October 2012 case study (dashed line): **(a)** for MLT1; **(b)** for MLT10.

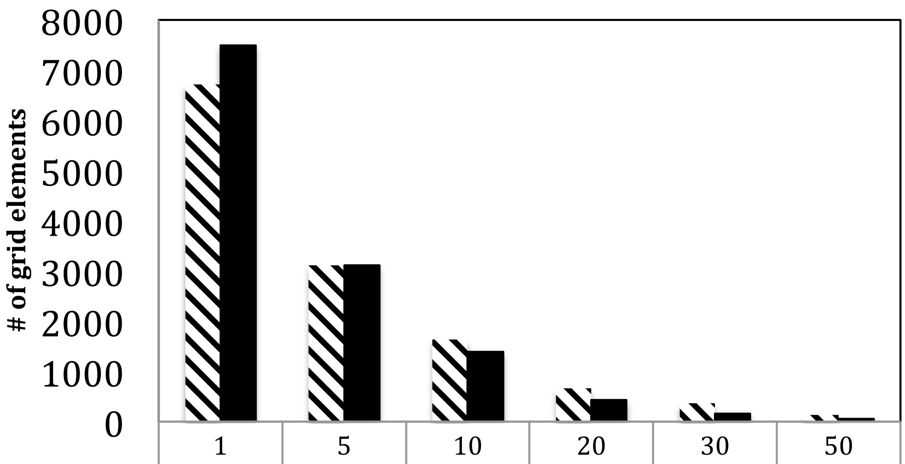

	1	5	10	20	30	50
RAMS	6717	3115	1638	662	363	126
LINET	7493	3115	1386	434	163	48

Fig. 13. Number of grid elements with a number of flashes greater or equal to a given threshold for the 5 km overlay and accumulated over all the case studies. The lightning thresholds are given in the x-axis (1, 5, . . . , 50 flashes per grid element).

NHESSD
2, 3351–3395, 2014